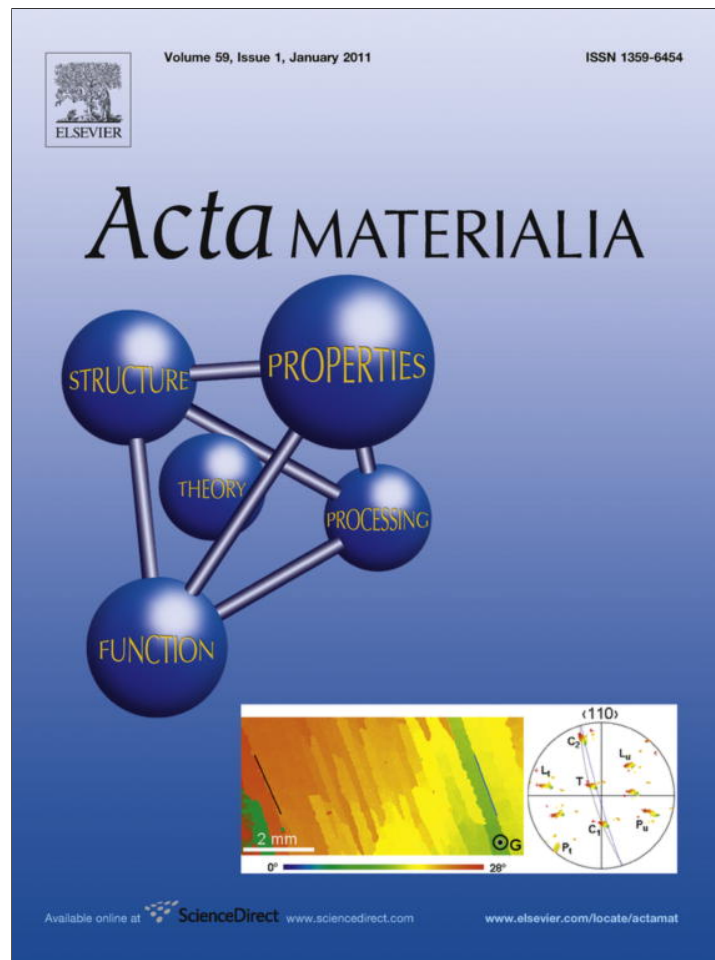


Provided for non-commercial research and education use.  
Not for reproduction, distribution or commercial use.



(This is a sample cover image for this issue. The actual cover is not yet available at this time.)

This article appeared in a journal published by Elsevier. The attached copy is furnished to the author for internal non-commercial research and education use, including for instruction at the authors institution and sharing with colleagues.

Other uses, including reproduction and distribution, or selling or licensing copies, or posting to personal, institutional or third party websites are prohibited.

In most cases authors are permitted to post their version of the article (e.g. in Word or Tex form) to their personal website or institutional repository. Authors requiring further information regarding Elsevier's archiving and manuscript policies are encouraged to visit:

<http://www.elsevier.com/copyright>



# Characterization and mechanical testing of alumina-based nanocomposites reinforced with niobium and/or carbon nanotubes fabricated by spark plasma sintering

K.E. Thomson<sup>a,1</sup>, D. Jiang<sup>a</sup>, W. Yao<sup>a</sup>, R.O. Ritchie<sup>b</sup>, A.K. Mukherjee<sup>a,\*</sup>

<sup>a</sup> Department of Chemical Engineering and Materials Science, University of California, Davis, CA 95616, USA

<sup>b</sup> Department of Materials Science and Engineering, University of California, Berkeley, CA 94720, USA

Received 12 April 2011; received in revised form 29 September 2011; accepted 2 October 2011

## Abstract

Alumina-based nanocomposites reinforced with niobium and/or carbon nanotubes (CNT) were fabricated by advanced powder processing techniques and consolidated by spark plasma sintering. Raman spectroscopy revealed that single-walled carbon nanotubes (SWCNT) begin to break down at sintering temperatures  $>1150$  °C. Nuclear magnetic resonance showed that, although thermodynamically unlikely, no  $\text{Al}_4\text{C}_3$  formed in the CNT–alumina nanocomposites, such that the nanocomposite can be considered as purely a physical mixture with no chemical bond formed between the nanotubes and ceramic matrix. In addition, in situ single-edge notched bend tests were conducted on niobium and/or CNT-reinforced alumina nanocomposites to assess their toughness. Despite the absence of subcritical crack growth, average fracture toughness values of 6.1 and 3.3  $\text{MPa m}^{1/2}$  were measured for 10 vol.% Nb and 10 vol.% Nb–5 vol.% SWCNT–alumina, respectively. Corresponding tests for the alumina nanocomposites containing 5 vol.% SWCNT, 10 vol.% SWCNT, 5 vol.% double-walled-CNT and 10 vol.% Nb yielded average fracture toughnesses of 3.0, 2.8, 3.3 and 4.0  $\text{MPa m}^{1/2}$ , respectively. It appears that the reason for not observing improvement in fracture toughness of CNT-reinforced samples is because of either damage to CNTs or possibly non-optimal interfacial bonding between CNT–alumina.

© 2011 Acta Materialia Inc. Published by Elsevier Ltd. All rights reserved.

**Keywords:** Nanocomposite; Carbon nanotubes; Alumina; Toughness; Raman spectroscopy

## 1. Introduction

The low density, chemical inertness and high hardness/strength of nanocrystalline alumina make it an attractive candidate for compressive structural applications. Unfortunately, its low fracture toughness ( $\sim 2.5$   $\text{MPa m}^{1/2}$ ) impedes its use in such applications. The most successful approach to improving alumina's fracture toughness has been the addition of second phases. The creation of ceramic–matrix composites (CMC) has combined the high strength/hardness of alumina and toughening from the second phases

by means of mechanisms such as ductile phase toughening, fiber toughening, transformation toughening and micro-crack toughening. Over the past decade, many researchers have studied the strengthening and toughening effects of adding various metal and ceramic phases to alumina [1–15]. Many researchers have explored the potentially beneficial effects of adding carbon nanotubes (CNT) to nanocrystalline alumina [16–31]. Unfortunately, the comparison of fracture toughness data is complicated by the fact that many different techniques have been used to assess the mechanical properties of these CMC. Specifically, many investigators employed the indentation fracture (IF) technique, which has been proved to be somewhat questionable for assessing the toughness of these materials [32].

The present work investigates the effect of adding CNT (single-walled (SWCNT) and double-walled (DWCNT))

\* Corresponding author. Tel.: +1 530 752 1776; fax: +1 530 752 9554.

E-mail address: [akmukherjee@ucdavis.edu](mailto:akmukherjee@ucdavis.edu) (A.K. Mukherjee).

<sup>1</sup> Present address: Stryker Endoscopy, 5900 Optical Court, San Jose, CA 95138, USA.

and elemental niobium on the mechanical properties of nanocrystalline alumina with the intent of creating a tough alumina-based nanocomposite. The intention was to examine whether the incorporation of CNT would provide a source of extrinsic toughening in alumina. CNT were chosen because, owing to their structural perfection, they are ultra-strong ( $\sim 0.15$  TPa [33]), yet at the same time flexible. In addition, their conductivity and relatively high-temperature resistance provide, in many respects, the ideal “nanocrystalline” fiber for reinforcement. Unfortunately, adequate dispersion of CNT is very difficult, owing to their tendency to group into “bundles” or “ropes” of 10–100 nanotubes (held together by weak Van der Waals forces) in order to minimize the surface area.

Second, it was proposed that niobium additions to nanocrystalline alumina would provide both intrinsic and extrinsic toughening via a ductile-phase toughening mechanism. Nb has been used as a model reinforcement, as it has been shown for many ceramic–matrix and intermetallic–matrix composites, where Nb has been incorporated in particulate form, that extrinsic toughening is particularly active. Niobium was also chosen because its high melting temperature would be compatible with the high-temperature sintering condition of alumina. Furthermore, the possible synergistic effect of combined toughening mechanisms, such as the ductile phase and fiber toughening, represents an exciting possibility in these materials.

To fabricate these materials, spark plasma sintering (SPS) was used for consolidation because it avoids the excessive grain growth that would prevent a truly nanocrystalline material from being obtained. SPS is an advanced, moderate pressure-assisted consolidation technique which can produce fully dense samples at lower temperatures and shorter times than conventional sintering techniques would allow. Although the mechanisms behind SPS are unclear, it is believed that a combination of rapid heating rate, pressure application and electrical pulsing enhances the surface diffusion and thus promotes sintering of ceramic powders [34,35].

## 2. Experimental methods

The details of processing conditions and parameters chosen for SPS of 5 vol.% SWCNT–alumina, 5 vol.% DWCNT–alumina, 10 vol.% Nb–alumina and 10 vol.% Nb–5 vol.% SWCNT–alumina are presented as a self-contained section in [Appendix](#).

### 2.1. Raman spectroscopy

Pulsed laser Raman spectroscopy was conducted at Lawrence Berkeley National Laboratory. Spectra were detected with an imaging photomultiplier ( $1024 \times 1024$ ) with  $5 \text{ cm}^{-1}$  resolution. First, an investigation into the preservation of 10 vol.% SWCNT–alumina consolidated at  $1150^\circ\text{C}$  for 3 min was conducted using lasers of 522–488 nm wavelength with a 60 s scan. Four scans were taken and overlaid

for comparison of D- and G-bands: pure SWCNT, graphite standard, pure alumina and the 10 vol.% SWCNT–alumina composite. Using the same equipment, a more in-depth Raman study was performed to identify the highest SPS condition that can be used without destroying the CNT. This experiment was conducted using a 488 nm  $\text{Ar}^+$  laser line at a power of 35 mW and collection times of 4 min.

### 2.2. Nuclear magnetic resonance

Nuclear magnetic resonance (NMR) was also used to investigate the CNT–alumina nanocomposites. Consolidated samples were crushed and sieved to yield powders fit for NMR study.  $^{27}\text{Al}$  magic angle spinning (MAS) NMR experiments were carried out on a Bruker Avance 500 wide-bore system, with Larmor frequency 130.32 MHz, MAS rate 15 kHz, digitization rate 166.7 kHz, pulse length  $0.5 \mu\text{s}$  ( $15^\circ$  tip angle) and 1 s of recycle delay, and transients of 1024. The system was calibrated with aluminum chloride solution, and  $\sim 100$  mg of powder was loaded into a 2.5 mm vial and analyzed under an 11.74 T magnetic field.

A series of spectra were taken to investigate the local chemical environment of alumina powder, as-received and subjected to high-energy ball-milling (HEBM), consolidated monolithic alumina and CNT–alumina composites in order to gain information about the interface between the CNT and the alumina matrix. All samples were sintered using 32 nm Nanotek alumina powder.

### 2.3. Mechanical testing

Vickers indentation methods were employed to determine the hardness and to estimate the approximate fracture toughness of the CMC in this study. A standard Tukon microhardness tester was used with a diamond Vickers tip, a 2.278 kg load and a dwell time of 12 s. In most cases, the hardness and toughness crack lengths were measured on a Buehler optical microscope with the Analysis program for maximum crack resolution. The indentation toughness was calculated using the Antis equation [36] by measuring both diagonal lengths and crack lengths. The average of the hardness and indentation toughness was taken from 10 or more indents.

Because the IF technique has been claimed to be questionable for assessing the toughness of these materials [32], single-edge notched four-point bend (SENB) tests were conducted using a standard servo-hydraulic MTS load frame with a 12.7 mm displacement cartridge and a 890 N load cartridge to provide a more appropriate characterization of the fracture toughness of the composites. Two  $3 \text{ mm} \times 4 \text{ mm} \times 19 \text{ mm}$  beams were cut from each SPS specimen and polished to a  $1 \mu\text{m}$  finish. Samples were first notched using a 0.5 mm diamond saw blade to a depth of  $\sim 600 \mu\text{m}$ ; final notches were created using a micro-notching procedure involving polishing the root of the machined notch using a razor blade with  $1 \mu\text{m}$  diamond paste; this technique reliably produced sharpened notches with a root

radius between 11 and 20  $\mu\text{m}$ . An optical microscope was used to measure the notch depth ( $a$ ) and notch radius of the beams. The final crack length to width ( $a/W$ ) ratios typically ranged from 0.2 to 0.3. LabView was used to conduct the four-point bending tests (load span 15 mm) under displacement control, and the breaking load was recorded. The beam fracture surfaces were analyzed by scanning electron microscopy (SEM) in a FEI XL-30 SFEG instrument.

In situ three-point bend testing was also conducted by SEM to measure the toughness while simultaneously imaging how the crack interacts with the material's microstructure; in this manner, extrinsic toughening effects, if any, of niobium and SWCNT additions to nanocrystalline alumina could be examined. SPS samples were polished to a 0.5  $\mu\text{m}$  surface finish and cut into beams with dimensions  $3 \times 4 \times 19$  mm. SENB samples were pre-notched using a diamond saw, followed by an automated razor blade with 1  $\mu\text{m}$  diamond paste to an  $a/W$  ratio of 0.25–0.5. Other sample preparation procedures were made in accordance with ASTM STP 1409. The pre-notched beams were three-point bend tested by SEM at a loading rate of  $0.55 \mu\text{m s}^{-1}$  within a Hitachi S-4300SE/N instrument, using a Gatan Microtest 2000 test assembly, and the process of crack propagation observed under back-scattering mode in an attempt to measure the crack-resistance curve ( $R$  curve). The fracture toughness of the nanocomposites was computed from the fracture load's breaking load using the stress intensity  $K$ -solutions given in ASTM E399. Fracture surfaces were analyzed in a FEI XL-30 SFEG SEM.

### 3. Results and discussion

#### 3.1. Raman spectroscopy

The results from the pulsed laser Raman spectroscopy are shown in Figs. 1 and 2. Comparison of the spectra in Fig. 1 for pure SWCNT with that of the nanocomposite consolidated at 1150  $^{\circ}\text{C}$  reveals a major peak at  $\sim 1595 \text{ cm}^{-1}$  and a shoulder in the  $1550\text{--}1575 \text{ cm}^{-1}$  region in both spectra.

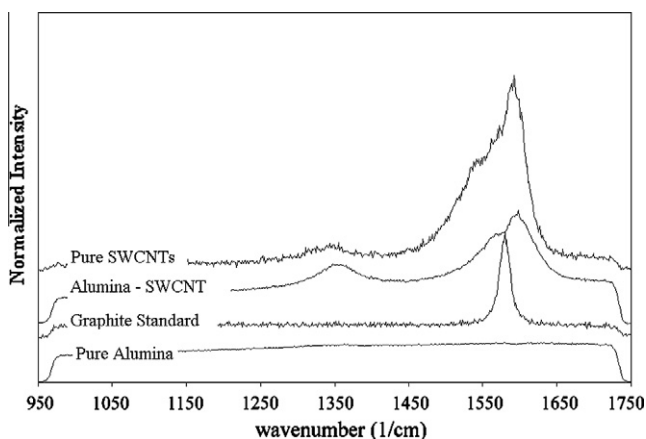


Fig. 1. Pulsed laser Raman spectroscopy comparing graphite, SWCNT and alumina starting powders with 10 vol.% SWCNT–alumina nanocomposite (SPS: 1150  $^{\circ}\text{C}$ , 3 min).

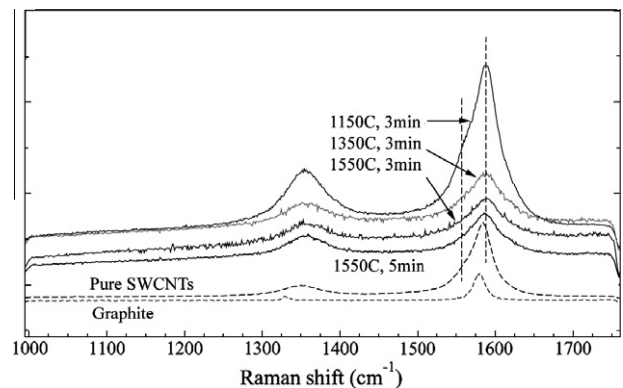


Fig. 2. Pulsed laser Raman study of SWCNT–alumina nanocomposites for determination of CNT degradation temperature as a function of SPS temperature and time [25].

This is termed the “G-band” and is the tangential shear mode of the carbon atoms. The “peak splitting” of this band reflects the overlap of electrons within the graphene layers when one rolls these sheets into tubes. Thus, although the graphite peak is located in the same position as the SWCNT spectrum, it does not have splitting or a shoulder. Therefore, the presence of splitting of the “G-band” indicates a nanotube structure. It should be pointed out that peak shift (in Raman spectroscopy) can also occur because of internal stress. In fact, in Fig. 2, the  $1580 \text{ cm}^{-1}$  (G-band) peak shift of the composite (the right dashed line) compared with pure SWCNT possibly indicates that a differential thermal contraction-related residual stress has developed in the composite after cooling down from the high sintering temperature. The minor peak at  $\sim 1350 \text{ cm}^{-1}$  is caused by defects and the presence of amorphous carbon and can be used to quantify the purity of processed CNT [25,37]. Clearly, the unique structure of CNT was intact after SPS consolidation at 1150  $^{\circ}\text{C}$  for 3 min.

A more in-depth Raman study was performed to identify the highest SPS condition that can be used without destroying the CNT. A series of spectra were taken with a 488 nm laser source at various laser powers ranging from 2.5 mW to 100 mW, as shown in Fig. 2. The same G-band peak splitting is seen in the lowest temperature spectra, representing consolidation at 1150  $^{\circ}\text{C}$ , as located by the left dashed line. One reviewer has pointed out that in Fig. 2, the shoulder in the G-band in the  $1550\text{--}1575 \text{ cm}^{-1}$  region (the left dashed line) for the specimen at 1150  $^{\circ}\text{C}$  for 3 min is hardly noticeable. Unfortunately, this lack of resolution is due to the data sampling scan time that was used. However, in Fig. 1, where a longer scan time was used, this shoulder on the G-band for the alumina–SWCNT (sintered at 1150  $^{\circ}\text{C}$ , 3 min) is clearly evident. Careful analysis of Fig. 2 shows that the peak splitting disappears in the spectrum, representing consolidation at 1350  $^{\circ}\text{C}$ , indicating the loss of the nanotube structure. Thus, CNT-reinforced CMC should be consolidated at temperatures below  $\sim 1250 \text{ }^{\circ}\text{C}$ . This is consistent with Flahaut et al.'s findings in in situ grown CNT–Fe–Alumina nanocomposites fabricated via hot pressing [17].

### 3.2. NMR

Analysis of the NMR spectra in Fig. 3 revealed that the aluminum atom coordination of the as-received powder was a mixture of four (at ~65 ppm) and six (at ~10 ppm). Close inspection of the sixfold peak indicates that there was some distortion in the aluminum–oxygen octahedral structure due to the small amount of splitting at the top of this peak. HEBM seems to provide sufficient energy to correct this distortion, because the HEBM spectra showed a clean sixfold peak (Fig. 3b). Consequently, consolidation in the SPS at 1200 °C results in complete phase transformation of the cubic 4-coordinated, metastable alumina gamma phase to the rhombohedral 6-coordinated, stable alpha phase as shown in Fig. 3c and d. Hence, after SPS consolidation, the sample had only alpha alumina, and all the mechanical tests were conducted on this alpha alumina matrix. The two satellite peaks in Fig. 3d are termed “spinning side bands” and are a result of spinning and are not indicative of the chemical environment of aluminum atoms.

In addition, analysis [42] of the CNT/alumina composite spectra for both 1200 °C and 1550 °C (not shown) indicated that the alumina remains 6-coordinated and that no aluminum carbide ( $\text{Al}_4\text{C}_3$ ) was formed. Although thermodynamically improbable because the reaction is very slow, a peak between 20 and 100 ppm would have appeared if aluminum carbide had been formed. The solid-state NMR equipment has sufficient sensitivity and, if this peak had been present, it would have been recorded. In other words, the composite sample was purely a physical mixture, and no chemical bonding occurred at the alumina grain/CNT interface. This is an important observation, because formation of  $\text{Al}_4\text{C}_3$

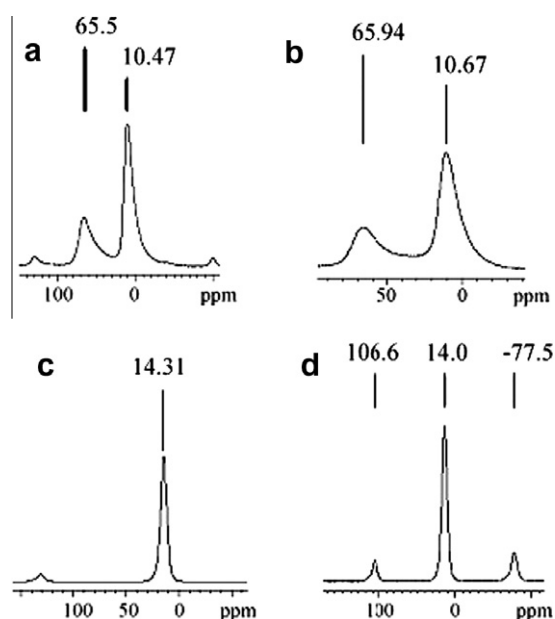


Fig. 3.  $^{27}\text{Al}$  MAS NMR spectra showing: (a) as-received alumina; (b) HEBM alumina; (c) pure alumina subjected to SPS at 1200 °C for 4 min; and (d) 5 vol.% SWCNT–alumina subjected to SPS at 1200 °C for 6 min (10–14 ppm = 6 coordinated and ~66 ppm = 4 coordinated).

would mean breakdown of the nanotube, because the nanotubes used in these studies were single-walled. Thus, it is clear that the nanotubes remained as ultra-strong reinforcing fibers within the brittle alumina matrix.

### 3.3. Mechanical testing

Although only approximate in the quantification of the fracture toughness, IF testing revealed anisotropy in crack lengths and, hence, some degree of extrinsic toughening in the CMC fabricated by SPS. For example, indents were introduced to both the cross-sectional and surface faces of the 10 vol.% Nb–alumina sample intermixed by cryomilling. The average IF toughness and hardness calculated on the cross-sectional surface (parallel to the pressing direction in SPS) was 3.5  $\text{MPa m}^{1/2}$  and 21.0 GPa, respectively. However, lower fracture toughness and slightly lower hardness were measured for the surface (perpendicular to the pressing direction in SPS), specifically 2.6  $\text{MPa m}^{1/2}$  and 20.8 GPa, respectively. This corresponds to a 32% difference in indentation toughness between the surface and cross-section orientations. The samples containing 5 vol.% DWCNT showed as much as 103% difference in indentation toughness when surface and cross-sectional indents were compared.

In addition, there was anisotropy found within the cross-sectional indents themselves. The cracks propagating in the pressing direction tended to be shorter than those perpendicular to the pressing direction, indicating maximum toughness in the pressing direction. Since the alumina grains were equiaxed, the anisotropic mechanical properties are attributed to residual stresses and, in the case of CMC, elongated niobium/CNT regions.

Table 1 shows all the data collected from four-point bend testing and Vickers indentation. Both surface (s) and cross-section surface (c.s.) were measured using Vickers indentation method. The data reveal that the samples made from the cryomilled Nb–alumina powders had slightly higher fracture toughness (by ~0.40  $\text{MPa m}^{1/2}$ ) than those made from the HEBM powder. The IF toughness values indicate that the same anisotropy seen in DWCNT CMC was also present in the cryomilled 10 vol.% Nb–alumina samples. Regardless of milling technique, the addition of 10 vol.% Nb to nanocrystalline alumina was more effective in improving the fracture toughness than CNT were. The Nb–alumina system contained less porosity (100% TD) and cleaner interfaces than the CNT system. The residual porosity (~1.5%) and the weakened alumina grain boundaries in the CNT system may explain the lack of toughening. Analysis of the indents made on the 10 vol.% Nb–alumina samples indicated that crack blunting was active and responsible for the improvement in fracture toughness.

Despite the increase in CNT loading, the 10 vol.% SWCNT samples displayed lower toughness than the 5 vol.% samples. Among the 10 vol.% SWCNT samples, the fracture toughness values increased from 2.45 to 2.76  $\text{MPa m}^{1/2}$  as the density increased from 96.4% to

Table 1  
Fracture toughness values determined from SENB bend testing and IF methods (where s and c.s. correspond to surface and cross-section surface).

	Density (% TD)	$K_{Ic}$ (MPa m <sup>1/2</sup> )	Hardness (GPa)	$K_{Ic}$ (IF) (MPa m <sup>1/2</sup> )
10 vol.% Nb–Al <sub>2</sub> O <sub>3</sub> Cryomilled, 60 min	100	3.94	s: 20.8 c.s.: 21.0	s: 2.6 c.s.: 3.4
HEBM, 24 h	100	3.52	s: 22.9	s: 3.3
5 vol.% DWCNT–Al <sub>2</sub> O <sub>3</sub>	98.5	3.3	s.: 20.4 c.s.: 19.0	s: 2.4 c.s.: 4.9
SWCNT–Al <sub>2</sub> O <sub>3</sub>				
5 vol.%	99.2	2.95	c.s.: 11	c.s.: 5.0
10 vol.%	97.4	2.76	n/a	n/a

97.4% TD. It is believed that the density of the samples outweighed the benefits of more reinforcing phase. Thus, obtaining full density in this material system is essential to obtain maximum strength and toughness.

Table 1 shows that DWCNT provided more toughening than the equivalent loading of SWCNT, i.e., 3.30 vs 2.95 MPa m<sup>1/2</sup>. The DWCNT sample also showed higher hardness, i.e., 19.0 vs 11 GPa. Conversely, the IF method predicted nearly identical fracture toughness for the two systems. This may be attributed to the difference in fracture surfaces, as shown in Fig. 4. The SWCNT appear to blanket the alumina grains in a weblike fashion. But even with micrometer-scale CNT agglomerates, the DWCNT–alumina nanocomposites appeared more homogeneous, and the CNT were well mixed with the alumina matrix. The ropes of DWCNT ran like tree roots into and out of the fracture surface.

Nanocrystalline alumina typically has a fracture toughness of 2.5–3.0 MPa m<sup>1/2</sup>. As shown in Table 1, no improvement in fracture toughness was measured when 5–10 vol.% SWCNT were added to alumina. All the values were within experimental error of that of pure alumina. Extrinsic toughening mechanisms, such as fiber bridging, are thought to be operable in the CNT–alumina nanocomposite system. Evidence of operation of such mechanisms was demonstrated earlier in the CNT–alumina system (Fig. 5). However, the fracture toughness values obtained in the current study suggest that these mechanisms are not able to improve the measured fracture toughness values, given the adopted testing method and the size of the test samples. Future work will employ the rising *R*-curve method to resolve this issue.

Although toughening was not quantified by fracture toughness results from SENB, a series of three-point bend testing was conducted inside an scanning electron microscope, with the objective of directly observing (qualitatively) extrinsic toughening mechanisms. Unlike materials that possess flat *R*-curves, the resistance to crack propagation actually increases as the crack length increases in *R*-curve materials such as silicon nitride, fiber-reinforced composites and coarse-grained alumina. In general, the resistance to crack propagation increases as the number of energy absorbing events increases in the crack wake.

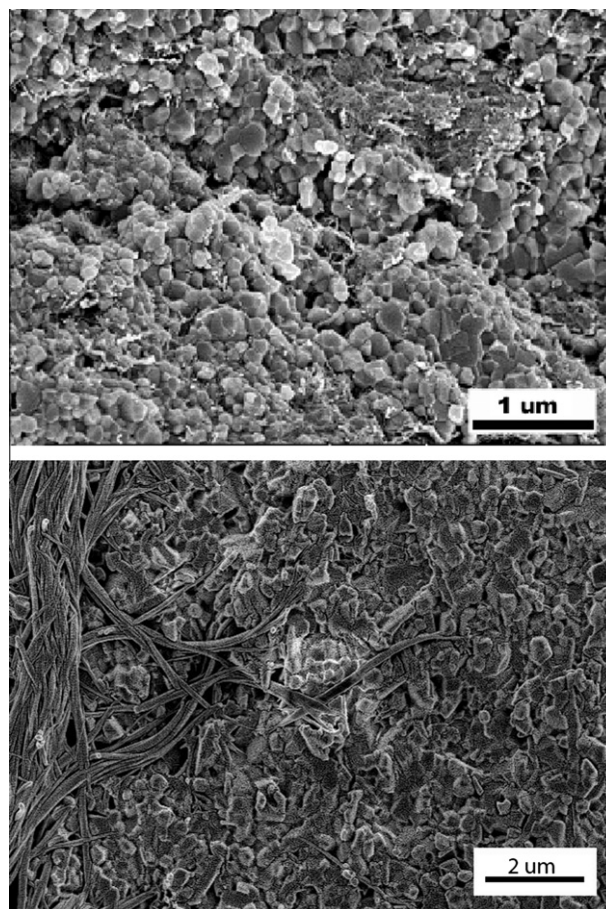


Fig. 4. SEM images of fracture surfaces of 5 vol.% SWCNT–alumina (top) and 5 vol.% DWCNT–alumina (bottom).

Table 2 displays the sintering parameters, data collected from the in situ three-point bend testing, and also the hardness/fracture toughness values obtained by the IF method. All the hardness and fracture toughness values given in Table 2 were calculated from the indents on the surface orientation (i.e., the indenter came down in the pressing direction). Although stable crack growth was not observed in these tests, the fracture toughness value obtained for 10 vol.% Nb–alumina from the breaking load was 6.1 MPa m<sup>1/2</sup>. This enhancement in fracture toughness is twice of that of monolithic alumina. However, the fracture

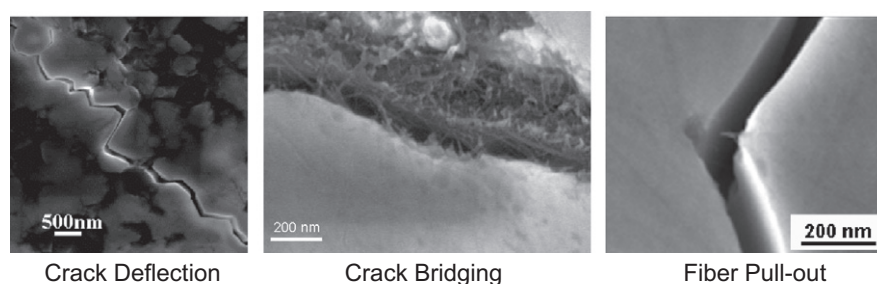


Fig. 5. SEM images illustrating the three ways in which fibers may toughen the alumina matrix by energy dissipation.

toughness of 10 vol.% Nb–alumina decreased to that of monolithic alumina when 5 vol.% SWCNT were added to the nanocomposite.

The 10 vol.% Nb–5 vol.% SWCNT–Al<sub>2</sub>O<sub>3</sub> nanocomposites possessed a slightly larger grain size than the Nb–Al<sub>2</sub>O<sub>3</sub> system, owing to the increase in SPS hold time, as noted in Table 2. The CNT were present in the alumina grain boundaries as well as between the niobium particles and the alumina matrix. Agglomerates of CNT ranged from tens of nanometers to a few microns in width, and there was evident porosity. The majority of cracks and pores were observed at the alumina–CNT interfaces, and crack bridging was seen in a few circumstances, as shown in Fig. 5.

Analyses of the post-mortem fracture surfaces indicate two distinct failure modes of the niobium particles. Both of which are apparent on the niobium particle in Fig. 6. First, some of the niobium regions completely debonded from the brittle alumina matrix. And in some cases, imprints of the small alumina grains can be seen in the region of debonding (indicated by the black arrow in Fig. 6). Second, it is apparent that the majority of the niobium particles tended to fracture in a brittle manner that is typical for body-centered cubic and high melting temperature metals such as niobium. Cleavage fracture and the presence of river lines indicate that the niobium particles ultimately failed without much plasticity. Such behavior is seen in the lower half of the niobium particle in Fig. 6.

The resulting bend fracture toughness of 6.1 MPa m<sup>1/2</sup> in the 10 vol.% Nb–alumina system indicates that the niobium regions did indeed absorb some energy from the propagating crack. Since this energy was not used to plastically deform the niobium, the crack propagation resistance is attributed to crack blunting and crack bridging. Such crack-tip shielding toughening mechanisms have been observed in Nb<sub>3</sub>Al composites reinforced with Nb particulate [38].

Observations and measurement of stable crack growth allow for the development of an *R*-curve. However, even with the smallest displacement rates, the three-point bend samples failed catastrophically. A bias-notched (cut diagonally) sample was also fabricated to allow for a decreasing *K*-field situation by creating a situation where the crack grew into an increasing wedge of material. The sample was tested under identical loading conditions, and no stable crack growth was observed [39].

However, upon analysis of the images taken before and after fracture, the crack that initiated failure was identified, and it was found that subcritical growth (and any observable *R*-curve behavior) occurred during the first 3 μm of crack growth. With a notch radius of ~30 μm, it is highly improbable that the exact region of failure could be identified and imaged with adequate resolution for *R*-curve development. It is concluded that nanocrystalline alumina is too brittle to allow for general *R*-curve measurement. Thus, for all practical purposes, nanocrystalline alumina reinforced with niobium or CNT does not show evidence of subcritical crack growth and hence *R*-curve behavior.

### 3.4. Comparative discussion

Inspection of the literature [16–31] reveals some inconsistencies among the groups studying CNT-reinforced alumina composites. For example, Fan et al. [21] fabricated 12 vol.% MWCNT–alumina composites and measured a fracture toughness of 5.5 MPa m<sup>1/2</sup>, whereas Wang et al. [23] reported a mere 3.3 MPa m<sup>1/2</sup> for the toughness of a nominally similar material (10 vol.% SWCNT–alumina). The densities (only 95%) and matrix grain sizes were similar; however, Fan et al. used a technique similar to that used in this study to make the DWCNT–alumina samples in order to disperse the CNT thoroughly, whereas Wang et al. simply mixed alumina and nanotube in the solution and then ball-milled. It is unlikely that the number of walls would

Table 2  
Summary of mechanical properties of in situ three-point bend study and IF method.

Composition	SPS parameters	Density (% TD)	Grain size	Indentation $K_c$ (MPa m <sup>1/2</sup> )	3pt Bend $K_{Ic}$ (MPa m <sup>1/2</sup> )	Hardness (GPa)
Al <sub>2</sub> O <sub>3</sub>	1300 °C/3 min	99.9	1.4 μm	2.7	3.1	20.9
10% Nb–Al <sub>2</sub> O <sub>3</sub>	1150 °C/3 min, 1300 °C/2 min	99.5	250 nm	3.3	6.1	22.9
10% Nb–5% SWCNT–Al <sub>2</sub> O <sub>3</sub>	1200 °C/5 min	98.4	580 nm	2.7	3.3	19.3

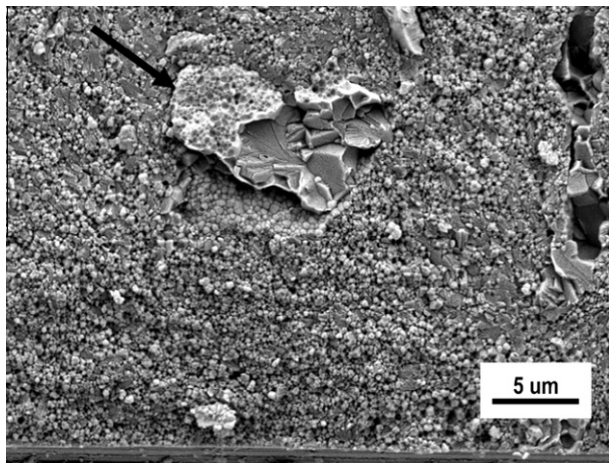


Fig. 6. SEM image of 10 vol.% Nb–Al<sub>2</sub>O<sub>3</sub> fracture surface (Au coated) displaying two modes of failure: particle debonding (arrow) and cleavage fracture.

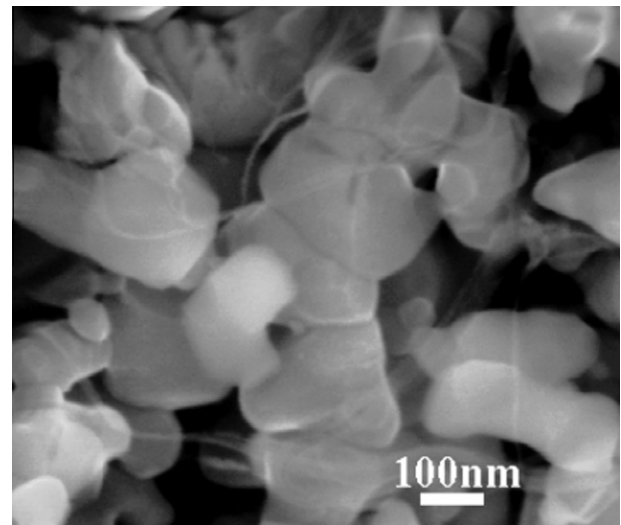


Fig. 7. High-resolution SEM image of an 86% dense 10 vol.% SWCNT–alumina sample showing little potential for load transfer and toughening from the nanotubes.

contribute to such a difference, but the fact that both groups had merely 95% dense specimens may explain the inconsistencies in results. However, it is clear from the CNT loadings reported that fully dense CNT–alumina composites are not easily obtained over ~10 vol.% CNT loading. This is also consistent with the present study's findings.

In 2003, some of the current authors published fracture toughness data for these composites based on the IF method [24], where a 200% increase in fracture toughness with incorporation of 10 vol.% SWCNT into nanocrystalline alumina was reported. These results were subsequently questioned by Wang et al. [23], who claimed to reproduce the Zhan et al. [24] study, but with contradictory results. Wang et al. employed both the IF and SENB techniques to measure the fracture toughness of 10 vol.% SWCNT–alumina, and they concluded that there was no benefit in adding CNT to alumina. However, it is clear from Table 3 that, since their SPS equipment/graphite die was limited to 40 MPa of applied stress, higher temperature and longer hold times were necessary to obtain high density. Consequently, their matrix grain size was thousands of nanometers, and they were able to obtain only a 95% dense sample—very unlike the microstructure originally reported on by Zhan et al., which was 100% dense.

The porosity and surface finish play very important roles in the mechanical properties of ceramics, particularly

hardness and IF toughness. It is clear from Fig. 7 that very little load transfer from the matrix to the CNT could be expected from an 86% dense sample. The standard for using the Vickers indentation method to quantify hardness specifically calls for finer than 1 μm surface finish and states that porosity may interfere with measuring indents properly. Fig. 8a is an image of Wang et al.'s Vickers indent on 10 vol.% SWCNT–alumina published in Ref. [23]. The surface finish of their composites was not acceptable for application of the Vickers method: large pores were present in the sample. The indentation load was accommodated by pore collapse, and no cracks evolved from the indent corners. In contrast, the nanocomposites fabricated by Zhan et al. possessed very little porosity, and the cracks emitted from the indent corners could easily be measured (Fig. 8b). The indentation load was clearly accommodated by pore collapse, and development of a radial crack was not possible.

In addition, the present study determined via Raman spectroscopy that the CNT begin to break down at temperatures >~1250 °C. To prove positively that Wang et al. could not expect to have retained the CNT in their samples, a sample was consolidated in the SPS at 1550 °C for 5 min. Fig. 2 clearly shows that there is no splitting of the G-band, and the intensities of the D- and G-bands grow more close

Table 3  
Comparison of Mukherjee vs Wang SWCNT–alumina investigation.

Comparison parameters	Mukherjee's group [24]	Wang et al. [23]
Starting materials	SWCNT + Al <sub>2</sub> O <sub>3</sub>	SWCNT + Al <sub>2</sub> O <sub>3</sub>
Dispersion and mixing methods	Wet-milling and sieving	No sieving
SPS processing conditions	SPS 1150 °C/3 min 63 MPa	SPS 1450–1550 °C/ 3–10 min, 40 MPa
Relative density	100	95.1
Grain size (nm)	~200	1000–2000
Fracture toughness	194% increase (IF)	No toughening (IF and SENB)

in amplitude, both signaling loss of CNT structure and creation of disordered graphite.

Furthermore, the present authors have tried to deliberately induce damage to CNT due to Joule heating by passing large pulsed current to the CNT/alumina powder compact [43] in the SPS process. The results revealed that the RBM peaks indexed by (11, 0), (9, 1) and (8, 0) chirality completely disappeared when a large current passed through the CNT. When BN spacers were used to isolate the top and bottom push-rods in the SPS equipment (thereby preventing any Joule heating in the CNT), no such loss of tubular chirality was noticed. These observations suggest that prior HEBM of the alumina powder and subsequent wet-milling of alumina powder and CNT with a dispersant did not affect the overall tubularity of CNT or damage the CNT. This wet-milling was conducted in a mild manner at a very low speed which would not result in any damage to CNT. However, subjecting the CNT to higher temperature in the sintering chamber (using high SPS temperature or passing a large current producing Joule heating) did produce damage.

As in the present study, Wang et al. also applied the SENB technique to measure fracture toughness. Unlike the discrepancies in the IF data, both groups obtained similar SENB results for 10 vol.% SWCNT–alumina; Wang et al. reported  $3.3 \text{ MPa m}^{1/2}$ , and the present study reports  $2.76 \text{ MPa m}^{1/2}$ . Interestingly, the 5 vol.% DWCNT–alumina samples tested with the SENB in the present study were exactly what Wang et al. measured ( $3.33 \text{ MPa m}^{1/2}$ ) for their 10 vol.% SWCNT–alumina samples. Consequently, most groups (including the present study) that have reported SENB fracture data have found that CNT–alumina composite materials have moderate or no increase in fracture toughness compared with the intrinsic toughness of monolithic alumina.

Fibers are added to matrices for strengthening and toughening via fiber bridging—a crack wake or extrinsic toughening phenomenon. Commonly, the amount of toughening increases with the volume content of fibers, because

the number of fibers bridging the crack wake increases as fiber loading increases. CNT were selected because they have a remarkable combination of tensile strength and flexibility. However, as depicted by the SENB testing, the inclusion of the CNT provided only a negligible contribution to the toughening. This may be attributed to the nanoscale nature of the CNT and/or a very weak interaction (i.e., negligible traction forces) between the nanotubes and alumina matrix. One reviewer suggested that, in general, a weak reinforcement/matrix interface is preferred for CMC. This follows because delamination along the interface permits the reinforcement (typically in the form of a fiber or whisker) to remain intact behind the crack tip to promote crack bridging. (Incidentally, this is not always the case where the reinforcement can itself deform—here an intermediate strength interface is preferable to promote maximum work done in deforming the reinforcement.) However, in the present work, the lack of a pronounced effect of the interface strength in the extent of toughening in CNT–alumina materials does indicate that either the effect of the CNT in generating crack bridging is minimal or that the CNT were damaged during processing. As there is little evidence of processing damage to the CNT, it is the present authors' strong belief that this effect results from a minimal role of crack bridging by the CNT. Strengthening the interface between the CNT and alumina by means of surface functionalization may result in some measurable extrinsic toughening. This phenomenon could theoretically be measured by methods that can achieve stable crack growth and obtaining an *R*-curve (stress intensity vs crack extension). *R*-curves can be obtained using standard bend testing or compact tension (C(T)) techniques, in which the load is incrementally increased during stable crack growth and the crack length recorded. From the recorded loads and crack measurements, the stress intensity *K* vs  $\Delta a$  (crack extension) curve can be generated.

Unfortunately, such stable crack growth is very difficult to obtain in nanocrystalline ceramics. In the present study, disk-shaped samples of pure alumina and 5 vol.%

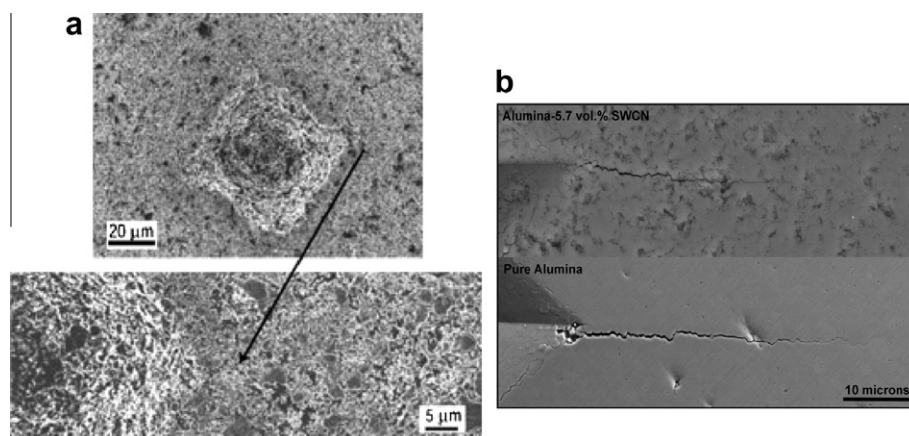


Fig. 8. Vickers indents from (a) Wang et al.'s paper [23] showing no crack generation on 10 vol.% SWCNT–alumina (95% dense) and (b) Zhan et al.'s paper [24].

SWCNT–alumina were tested using the C(T) technique (ASTM 399). Stable crack growth, and, hence, development of an *R*-curve, could not be obtained in either system. It is clear that the nanocrystalline alumina matrix was simply too brittle to measure the extrinsic toughening expected from grain and fiber bridging.

It is clear that, with respect to the fracture toughness of CNT reinforced ceramic composites, comparison of results from various investigators in the literature [1–31] should be performed with some caution, as the different methods used to evaluate the fracture toughness, specifically the indentation toughness and standard precracked bend or C(T) methods, can yield conflicting results. In particular, the indentation method (IF) of estimating the fracture toughness can be misleading and inaccurate in these particular materials.

#### 4. Conclusions

Alumina-based nanocomposites were successfully fabricated using advanced powder processing techniques (i.e., HEBM and cryomilling) and consolidated using SPS. In just a few minutes, fully dense (>98.5% TD) niobium and/or CNT-reinforced alumina nanocomposites were produced. Raman spectroscopy was used to verify that the nanotubes were preserved after sintering within the SPS at 1150 °C. However, it was also found that SWCNT are destroyed if sintered at 1350 °C. Thus, it is advised that consolidation temperatures be limited to ~1250 °C when SWCNT are present within the sample. NMR showed that no  $Al_4C_3$  was formed in SWCNT–alumina nanocomposites, even after consolidation at 1500 °C for 10 min. Thus, the SWCNT–alumina is purely a physical mixture, and no chemical bonding occurs between the CNT and alumina. The structural perfection of SWCNT have not been compromised, and they remain as ultra-strong fibers.

SPS results in anisotropic mechanical properties in alumina nanocomposites due to residual stresses and preferential alignment of CNT or Nb agglomerates perpendicular to the pressing direction. A 103% difference in fracture toughness between sample orientations (surface vs cross section) was measured using the Vickers indentation method in the 5 vol.% DWCNT–alumina samples. Using single-edge V-notched bend testing to measure the toughness of alumina-based nanocomposites, the fracture toughness of 5 and 10 vol.% SWCNT–alumina composites was found, within experimental error, to be comparable with that of pure alumina (~3 MPa m<sup>1/2</sup>). Similarly, samples consolidated from cryomilled and HEBM powders had an average fracture toughness of 3.9 and 3.5 MPa m<sup>1/2</sup>, respectively. Note though that CNT can be added to nanocrystalline alumina to induce beneficial of anisotropic electrical and thermal properties [40,41] without degrading the toughness. Additions of 10 vol.% Nb, however, was successful in toughening nanocrystalline alumina, yielding a toughness of ~6 MPa m<sup>1/2</sup> measured in three-point bend tests. For both CNT- and Nb-reinforced nanocrystalline

alumina, no subcritical crack growth could be detected, owing to the extreme brittleness of the matrix alumina; consequently, neither class of composites was found to display resistance-curve behavior, which is a characteristic of active extrinsic toughening mechanisms.

Controversy remains about the effectiveness of CNT additions to the toughening of alumina. In this work, it is found that indentation toughness and SENB tests of CNT-reinforced nanocrystalline alumina composites both show that reinforcement by the nanotubes provides only minimal increases in the fracture toughness. However, as previous experiments using indentation toughness measurements have shown widely conflicting results, it is concluded that this latter technique is highly questionable for estimating the toughness of these materials, and it is suggested that future toughness evaluations should be performed using standard precracked or sharply notched samples.

#### Acknowledgements

This investigation was supported by a Grant from the US Army Research Office (#W911NF-04-1-0348) and a Grant from the US National Science Foundation (#NSF-CMMI-0700272) to the Department of Chemical Engineering and Materials Science of the University of California, Davis (through AKM). The involvement of ROR was supported by the Office of Science, Office of Basic Energy Sciences, Division of Materials Sciences and Engineering, of the US Department of Energy under Contract No. DE-AC02-05CH11231. The authors would like to thank an anonymous reviewer for constructive comments.

#### Appendix A. Processing details

##### A.1. 5 vol.% SWCNT–Alumina

The as-received nanocrystalline alumina powder was first subjected to HEBM. Total powder charges of ~10 g of powder were loaded into a tungsten carbide (WC) vial with a single 14.3 mm WC ball and subjected to HEBM for 24 h in a Spex 8000 Mixer/Mill. To prevent severe powder agglomeration during milling, 1 wt.% polyvinyl alcohol (PVA) was added, but was baked out at 350 °C for 3 h in air before further processing was performed. To prevent the natural tendency of CNT to agglomerate, due to Van der Waals forces, 10 mL of Nanospense (made by NanoLab) was added to ~200 mL of deionized (DI) water and mixed by hand until dissolved. The appropriate amount of SWCNT produced via the HiPco method (Carbon Nanotechnologies, Inc., Texas, ~1–4 nm diameter, 90% purity) was added to the dispersant solution and in ultrasonication for ~15 min. Simultaneously, the appropriate amount of HEBM alumina powder (NanoTek, 32 nm) was added to ~200 mL of ethanol, hand stirred and in ultrasonication for ~5 min. The composite slurry was added to a polystyrene bottle with ~25 vol.% zirconia ball

media and wet-milled for 24 h. The solvent was then evaporated off on a stirring hot plate. The dispersant was baked off at 400 °C for 3 h in air before SPS consolidation. The SPS conditions were 1200 °C for 5–8 min under 25 kN load (88 MPa) and resulted in samples with relative densities from 97.7% to 98.3%.

#### A.2. 5 vol.% DWCNT–alumina

Sodium dodecyl sulfate (SDS) and polyethylene glycol with a molecular weight of 2000 (PEG 2000) were used as dispersants for the DWCNT and nanocrystalline alumina, respectively. A 1 wt.% SDS solution was created in 300 mL of DI water and 0.49 g of DWCNT was added and ultrasonicated for 15 min. The DWCNT (NanoLab, OD  $4 \pm 1$  nm, 1–5  $\mu$ m length, >90% purity) were produced by chemical vapor deposition. Simultaneously, a 0.5 wt.% PEG 2000 solution was made with 300 mL of DI water, and 19.51 g of HEBM alumina (CR30, Baik-alox Corp., grain size  $\sim 45$  nm) was added and ultrasonicated for 15 min. The two slurries were slowly combined while stirring by hand and ultrasonicated for an additional 5 min. The composite slurry was added to a polystyrene bottle with  $\sim 25$  vol.% zirconia ball media and wet-milled for 24 h. The solvent was evaporated off on a stirring hot plate. The SDS and PEG 2000 were baked out of the powder by the following heat treatment: 1.5 h at 150 °C, 1.5 h at 400 °C, 12 h at 450 °C in air, 4 h at 600 °C in Ar, and finally 3 h at 850 °C in Ar. The agglomerated powders were then crushed and sieved to 150  $\mu$ m and consolidated via SPS. Dense (98.5% TD) samples were obtained by SPS at 1250 °C for 3 min under 30 kN load (105 MPa).

#### A.3. 10 vol.% Nb–alumina

In order to investigate the effectiveness of both HEBM and cryomilling, the 10 vol.% Nb–alumina system was used to compare the two techniques. The following powders were mixed by hand prior to HEBM and cryomilling: as-received alumina powder ( $\alpha$  and  $\gamma$  phases, 45 nm, Baikowski International Corp.), the appropriate amount of 90 wt.% Nb (99.85% purity, 74  $\mu$ m, Goodfellow)–10 wt.% Al (99.5% purity, 45  $\mu$ m, Johnson Matthey Electronics) alloy to yield a 10 vol.% Nb/alumina composition, and 1 wt.% PVA. Aluminum was added to reduce the surface oxide of the niobium particles, and PVA was added to prevent severe powder agglomeration. This powder mixture was subjected to HEBM (Spex 8000 Mixer/Mill) for 24 h or cryomilled (Spex 6700 Freezer Mill) for 60 min. The composite powders were heat treated (350 °C for 3 h in vacuum or Ar) to remove the PVA without oxidizing the niobium. Fully dense samples (100% TD) were obtained after SPS at 1300 °C for 3 min under 30 kN pressure (105 MPa).

#### A.4. 10 vol.% Nb–5 vol.% SWCNT–alumina

The HEBM 10 vol.% Nb–alumina composite powder from above was ultrasonicated for 15 min in 500 mL of ethanol. The slurry was then added to a polypropylene bottle with 280 g ( $\sim 1/3$  by volume) of zirconia ball media and wet-milled (130 rpm) for 24 h. The appropriate amount of SWCNT ( $\sim 90\%$  purity, Carbon Nanotechnologies, Inc., Texas) was weighed out and added to a solution of 8 mL of Nanospense (an organic surfactant made by NanoLab) and 150 mL of DI water. During the final minutes of the previously mentioned wet-milling, the SWCNT/Nanospense aqueous solution was ultrasonicated for 5 min. The wet-milled slurry was slowly added to the dispersed CNT solution while ultrasonating and was added back into the polypropylene bottle and wet-milled for an additional 24 h.

The Nb/SWCNT/alumina slurries were taken off the wet-mill, ball-media separated, sieved through a 150- $\mu$ m mesh, and placed in a medium-sized glass beaker. A magnetic stir bar was added, and the slurry was dried on a stirring hotplate. Once dry, the agglomerates were broken up with a mortar and pestle and sieved through 150- $\mu$ m mesh. In the case where Nanospense was used, the dispersant was baked off at 450 °C for 4 h. The powders were consolidated with SPS into samples 3–4 mm thick at 1200 °C for 5 min under 30 kN load (105 MPa).

## References

- [1] Tuan WH, Brook RJ. *J Eur Ceram Soc* 1990;6:31.
- [2] Ji Y, Yeomans JA. *J Eur Ceram Soc* 2002;22:1927.
- [3] Mishra RS, Mukherjee AK. *Mater Sci Eng A* 2001;301:97.
- [4] Garcia DE, Schicker S, Bruhn J, Janssen R, Claussen N. *J Am Ceram Soc* 1998;81:429.
- [5] Diaz LA, Valdes AF, Diaz C, Espino AM, Torrecillas R. *J Eur Ceram Soc* 2003;23:2829.
- [6] Nawa M, Sekino T, Niihara K. *J Mater Sci* 1994;29:3185.
- [7] Sekino T, Nakajima T, Ueda S, Niihara K. *J Am Ceram Soc* 1997;80:1139.
- [8] Kim YD, Oh ST, Min KH, Jeon H, Moon IH. *Scripta Mater* 2001;44:293.
- [9] Oh ST, Sekino T, Niihara K. *J Eur Ceram Soc* 1998;18:31.
- [10] Rousset A. *J Solid State Chem* 1994;111:164.
- [11] Qin XY, Cao R, Li HQ. *Ceram Int* 2006;32:575.
- [12] Anya CC. *J Mater Sci* 1999;34:5557.
- [13] Zhu WZ, Gao JH, Ding ZS. *J Mater Sci* 1997;32:537.
- [14] Acchar W, Cairos CA, Segadaes AM. *Mater Sci Eng A* 2005;406:74.
- [15] Sarkar D, Adak S, Mitra NK. *Compos Part A – Appl Sci Manuf* 2007;38:124.
- [16] Cha SI, Kim KT, Lee KH, Mo CB, Hong SH. *Scripta Mater* 2005;53:793.
- [17] Flahaut E, Peigney A, Laurent C, Marliere C, Chastel F, Rousset A. *Acta Mater* 2000;48:3803.
- [18] Sun J, Gao L, Jin XH. *Ceram Int* 2005;31:893.
- [19] Mo CB, Cha SI, Kim KT, Lee KH, Hong SH. *Mater Sci Eng A* 2005;395:124.
- [20] An JW, You DH, Lim DS. *Wear* 2003;255:677.
- [21] Fan JP, Zhao DQ, Wu MS, Xu ZN, Song J. *J Am Ceram Soc* 2006;89:750.

- [22] Siegel RW, Chang SK, Ash BJ, Stone J, Ajayan PM, Doremus RW, et al. *Scripta Mater* 2001;44:2061.
- [23] Wang XT, Padture NP, Tanaka H. *Nat Mater* 2004;3:539.
- [24] Zhan GD, Kuntz JD, Wan JL, Mukherjee AK. *Nat Mater* 2003;2:38.
- [25] Jiang DT, Thomson K, Kuntz JD, Ager JW, Mukherjee AK. *Scripta Mater* 2007;56:959.
- [26] Yamamoto G, Omori M, Hashida T, Kimura H. *Nanotechnology* 2008;19.
- [27] Wei T, Fan ZJ, Luo GH, Wei F. *Mater Lett* 2008;62:641.
- [28] Ahmad K, Pan W. *Compos Sci Technol* 2008;68:1321.
- [29] Zhang T, Kumari L, Du GH, Li WZ, Wang QW, Balani K, et al. *Compos Part A – Appl Sci Manuf* 2009;40:86.
- [30] Ahmad I, Cao HZ, Chen HH, Zhao H, Kennedy A, Zhu YQ. *J Eur Ceram Soc* 2010;30:865.
- [31] Bi S, Hou G, Su X, Zhang Y, Guo F. *Mater Sci Eng A* 2011;528:1596.
- [32] Quinn GD, Bradt RC. *J Am Ceram Soc* 2007;90:673.
- [33] Demczyk BG, Wang YM, Cumings J, Hetman M, Han W, Zettl A, et al. *Mater Sci Eng A* 2002;334:173.
- [34] Chen W, Anselmi-Tamburini U, Garay JE, Groza JR, Munir ZA. *Mater Sci Eng A* 2005;394:132.
- [35] Shen ZJ, Johnsson M, Zhao Z, Nygren M. *J Am Ceram Soc* 2002;85:1921.
- [36] Anstis GR, Chantikul P, Lawn BR, Marshall DB. *J Am Ceram Soc* 1981;64:533.
- [37] Saito R, Dresselhaus G, Dresselhaus MS. In: Saito R, Dresselhaus G, Dresselhaus MS, editors. *Physical properties of carbon nanotubes*. London: Imperial College Press; 1998.
- [38] Bencher CD, Sakaida A, Rao KTV, Ritchie RO. *Metall Mater Trans A* 1995;26:2027.
- [39] Thomson KE, Jiang D, Lemberg JA, Koester KJ, Ritchie RO, Mukherjee AK. *Mater Sci Eng A* 2008;493:256.
- [40] Zhan GD, Mukherjee AK. *Rev Adv Mater Sci* 2005;10:185.
- [41] Zhan GD, Kuntz JD, Mukherjee AK, Zhu PX, Koumoto K. *Scripta Mater* 2006;54:77.
- [42] Thomson KE. *Processing, characterization and mechanical properties of alumina-based nanocomposites*. PhD dissertation, University of California, Davis; 2007.
- [43] Huang Q, Jiang D, Ovid'ko IA, Mukherjee AK. *Scripta Mater* 2010;63:1181.